Available online at www.sciencedirect.com

ScienceDirect

Proceedings of the Combustion Institute 39 (2023) 5347–5356

Proceedings of the Combustion Institute

www.elsevier.com/locate/proci

A novel reduced-order model method for characterization of acoustic response of laminar premixed flames

Zheng Qiao [a], Yu Lv [b,*]

[a] Department of Aerospace Engineering, Mississippi State University, Mississippi State, MS 39762, USA
[b] State Key Laboratory of Nonlinear Mechanics, Institute of Mechanics, Chinese Academy of Sciences, Beijing 100080, China

Received 5 January 2022; accepted 28 July 2022
Available online 22 September 2022

Abstract

This study presents a general, predictive and cost-efficient reduced-order modeling (ROM) technique for characterization of laminar premixed flame response under acoustic modulation. The model is built upon the kinematic flame model–G-equation to describe the flame topology and dynamics, and the novelties of the ROM lie in *i*) a procedure to create the compatible base flow that can reproduce the correct flame geometry and *ii*) the use of a physically-consistent acoustic modulation field for the characterization of flame response. This ROM addresses the significant limitations of the classical kinematic model, which is only applicable to simple flame configurations and relies on ad-hoc models for the modulation field. The ROM is validated by considering the acoustically-excited laminar premixed methane/air flames in conical and M-shape configurations, experimentally study by Durox et al. *Proc. Combust. Inst.*, 32 (2009). To test the model availability to practical burners, a confined flame configuration Cuquel et al., *Proc. Combust. Inst.*, 34 (2013) is also employed for model evaluation. The model accuracy is evaluated concerning flame geometrical features and flame describing function, and assessed by comparing the ROM results with both the experimental measurements and the direct-numerical-simulation results. It is found that the flame describing/transfer functions predicted by the ROM compare well with reference data, and are more accurate than those obtained from the conventional kinematic model built upon heuristically-presumed modulation fields.

Keywords: G-equation; Linear analysis; Flame describing function; Acoustic modulation; Reduced-order model

1. Introduction

Over the past decade remarkable progress has been accomplished toward enabling predictive analysis of combustion instability for real-world applications [1,2]. Full-scale high-fidelity simulation has been applied to characterize the unsteady combustion behaviors in realistic engine geometries. However, due to the high computational cost, the applicability of this technique, in particular to a broad range of operability map, remains very lim-

* Corresponding author.
E-mail address: lvyu@imech.ac.cn (Y. Lv).

https://doi.org/10.1016/j.proci.2022.07.229
1540-7489

ited. As an efficient and versatile alternative, the theoretical framework based on the flame describing function (FDF) [3,4] has recently gained increasing attentions. In this theory, the FDF plays a vital role, which represents the flame response to local flow disturbance in a mathematical form of :

$$\mathcal{F}\left(\frac{\hat{u}}{U_0}, f\right) = \frac{\hat{\dot{Q}}(\hat{u}/U_0, f)/\bar{\dot{Q}}}{\hat{u}(f)/U_0} = G\left(\frac{\hat{u}}{U_0}, f\right) e^{i\varphi\left(\frac{\hat{u}}{U_0}, f\right)}, \quad (1)$$

where $\hat{u}$ is the velocity perturbation amplitude at the flame holder and $\hat{\dot{Q}}$ is the Fourier transform of the induced heat-release-rate fluctuation; accordingly, G and φ are the gain and phase delay, and both are bivariate functions of frequency f and perturbation level $\hat{u}(f)/U_0$. FDF can be coupled with analytical acoustic models [5,6] or thermoacoustic solvers [7] to effectively predict the combustion modalities and characterize the nonlinear thermoacoustic behaviors of combustion devices [2]. However, the successful analysis is essentially dependent on the accurate evaluation of FDF. In practice, FDF is either measured via experiment or evaluated using numerical simulation.

With regard to the computational determination of FDF, it is either by means of high-fidelity but very time-consuming techniques, such as large-eddy simulation [8–10], or based on efficient but low-order models (ROM), such as the kinematic models with G-equation [3,11–15] and the linearized Navier-Stokes (LNS) equations [13,16]. The main issue associated with the ROM technique is that it is only limited to simple flame configurations, e.g., conical or slot flame, where the base-flow knowledge is well understood, and the presumed perturbation flow field reasonably reflects the true physics.

To improve the fidelity of ROM technique and remove the ad-hoc assumptions, there are recent efforts [13,17,18] devoted to developing physically-informed velocity perturbation fields. These modeling efforts focus on the accurate description of the feedback between the flame and flow responses. As exhibited in the experimental studies of Baillot et al. [19] and Birbaud et al. [20], this feedback mechanism plays an active role in producing convective perturbation mode. Blanchard et al. [13] applied LNS analysis to a M-shape flame and identified the vorticity generated at the flame front as a driving mechanism for convective perturbation mode. To account for the vortical mode, in their ROM the wrinkled flame sheet is modeled as a vorticity sheet driven by the effects of localized curvature and local strain. Steinbacher et al. [18] identified for a 2D slit flame that the vorticity generated by baroclinic torque at the flame front is the source of convective perturbation mode in the flame cone. They proposed another ROM by modeling the convective perturbation subject to this particular vorticity generation mechanism. Despite the progress made in modeling the velocity perturbation field in physics-based methods, several issues remain to be addressed. For instance, although the flame-flow feedback interaction is accounted for, but the accurate model for hydrodynamic and thermo-diffusive modes (linear) has not been incorporated into these ROMs. Moreover, the ROMs in [13,18] are both built upon the linearized G-equation, and therefore cannot capture the nonlinear response resulting from the flame disturbance itself. In this regard, the above-mentioned ROMs may be used to predict FTF (flame transfer function-the FDF with small amplitude perturbations). The efficient ROM that can provide predictive FDF has yet to be developed. The present effort is taken toward addressing this need.

In the study, a reduced-order model will be proposed upon the basis of the kinematic model that *solely* solves the nonlinear G-equation to track laminar flame front and delineate heat release behavior (as the integral of flame surface [4]). In order to fundamentally address the existing model limitation and improve the model fidelity, we will present a novel procedure to construct the modulating flow field that allows the laminar flame front to evolve in the physically-consistent manner. To this end, the necessary flow information will be derived from the base-flow of the combustion field through linearized flow analysis. The base-flow will be taken from the steady flame solution of detailed simulation in the present study, but could also be obtained from experimental study or Reynolds-Averaged Navier-Stokes simulation. It will be shown that with the embedded critical physical knowledge the resulting ROM is capable of capturing the laminar flame response to flow perturbations and delivering predictive FDF results, even though the flame-flow feedback effect is not taken into account.

The content of this paper is organized as follows. The ROM solution techniques are detailed in Section 2 The validation study is carried out in Section 3 to assess the accuracy of the proposed ROM by considering different laminar premixed flame configurations. The flame response predictions will be compared against experimental data and DNS solutions. Section 4 extends the application to a confined flame setting to further evaluate the model generality. The paper finishes with conclusions in Section 5.

2. Solution techniques

The calculation procedure of the presented ROM is illustrated in Fig. 1 and summarized as follows: First, perform the direct simulation for the steady (unperturbed) flame, for which the computational details are given in Sec. 2.1. Then, con-

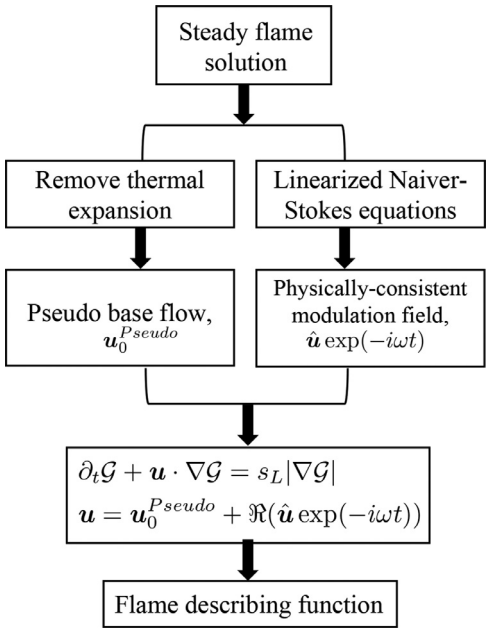

Fig. 1. Workflow and calculation procedure of the reduced-order modeling approach for characterization of flame response to acoustic modulation.

struct a pseudo base flow following the method proposed in Sec. 2.2. This step is a one-time effort for a given configuration. Meanwhile, carry out the linear input-output analysis, as discussed in Sec. 2.3, using the steady flame solution as the base flow to obtain an accurate acoustic-modulation field at different frequencies. The obtained modal solution is transformed to time domain, which is then superimposed onto the pseudo base flow to form the actual flow field used in G-equation based kinematic model. For a given set of frequency and perturbation levels, the G-equation is solved with the approach in Sec. 2.4 to predict the flame response. To obtain FTF (flame transfer function the FDF with a very small amplitude) or FDF, one only needs to repeat the G-equation calculation until the relevant ranges of frequency and amplitude are swept.

2.1. Direct numerical simulation (DNS)

The variable-density reacting flow is described by the Navier-Stokes equations at the low-Mach limit:

$$\partial_t \rho + \nabla\cdot(\rho\vec{)} = 0\,, \tag{2a}$$

$$\partial_t(\rho\boldsymbol{u}) + \nabla\cdot(\rho\boldsymbol{u}\boldsymbol{u}^T) = -\nabla p + \nabla\cdot\boldsymbol{\tau}\,, \tag{2b}$$

$$\rho c_p\partial_t T + \rho c_p\boldsymbol{u}\cdot\nabla T = \nabla\cdot(\lambda\nabla T) - \sum_i^N h_i\dot{\omega}_i\,, \tag{2c}$$

$$\rho\partial_t Y_i + \rho\boldsymbol{u}\cdot\nabla Y_i = \nabla\cdot(\rho D\nabla Y_i) + \dot{\omega}_i\,, \tag{2d}$$

$$\rho = f_{EOS}(T, Y_i)\,, \tag{2e}$$

in which ρ, $\boldsymbol{u}$, $\boldsymbol{t}$, p, T, Y, h, and c_p are density, velocity, viscous stress tensor, pressure, temperature, species mass fraction, specific enthalpy, and heat capacity at constant pressure, respectively; and $\dot{\omega}$ refers to the chemical production rate of the species. The mass diffusivity takes the form of $D = \mu/(\rho\mathrm{Sc})$, where the Schmidt number, Sc, is set to 0.7 and the dynamic viscosity, μ, is described with the classical power law. The thermal conductivity, λ, is determined via $\lambda = c_p\mu/\mathrm{Pr}$ with a Prandtl number of 0.7. In this study, the methane/air combustion is modeled with a one-step global reaction: $CH_4 + 2O_2 \longrightarrow CO_2 + 2H_2O$. The reaction rate, $\dot{\Omega}$, is expressed by the Arrhenius law,

$$\dot{\Omega} = A\left[\frac{\rho Y_{\mathrm{CH_4}}}{W_{\mathrm{CH_4}}}\right]^{n_{\mathrm{CH_4}}}\left[\frac{\rho Y_{\mathrm{O_2}}}{W_{\mathrm{O_2}}}\right]^{n_{\mathrm{O_2}}}\exp\left(-\frac{E_a}{RT}\right) \tag{3}$$

with the pre-exponential factor $A = 2.119\times 10^{11}\ \mathrm{m}^{1.5}/\left(\mathrm{s}\cdot\mathrm{mol}^{0.5}\right)$, the activation energy $Ea = 2.027\times 10^8\ \mathrm{J}\cdot\mathrm{mol}^{-1}$, $n_{\mathrm{CH_4}} = 0.2$ and $n_{\mathrm{O_2}} = 1.3$. This set of equations are solved, following the procedure by Pierce [21] with a second-order finite-difference scheme on a staggered grid and a third-order Runge-Kutta (RK) time-stepping scheme, for the direct numerical simulations. A uniform velocity profile is imposed at the inlet; zero pressure gradient is prescribed at the outlet. The nozzle walls are treated as non-slip, isothermal walls while the confined walls are treated as non-slip, adiabatic walls. Such simulations are performed in 2D axisymmetric domains, and used to generate the steady-state flame profile for the ROM and also the reference unsteady-flame solutions for validation study.

2.2. Pseudo base-flow

In this section the discussions focus on why and how to construct the pseudo base flow indicated in Fig. 1 for our G-equation based ROM. It should be pointed out that evolving the G-equation requires a complete and model-compatible flow field. Directly using the steady flow field of reactive DNS is not an option for our purpose, because the level-set solution cannot stabilize in the significantly accelerated flow in the post-flame region, which is induced by the thermal expansion across the flame. The same problem was also encountered in previous studies. To circumvent this issues, researchers suggested to use the uniform flow for conical flames [22], and resorted to the potential flow model or RANS results [15] for M-shape flames. Here we propose a more general and parameter-free approach for this purpose. The key idea is to construct the pseudo

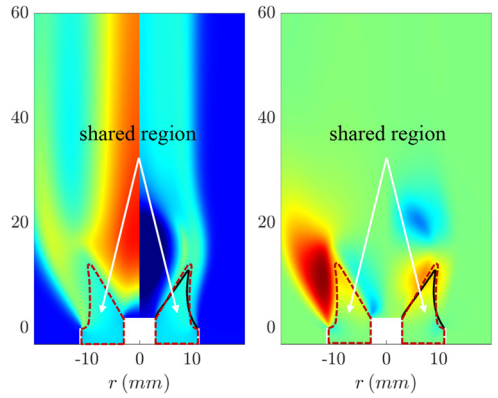

(a) streamwise velocity field (b) radial velocity field

Fig. 2. DNS flow field versus the constructed pseudo base flow illustrated in a M-shape flame setting, including the streamwise (a) and radial (b) velocity fields. In each panel, the left and right contourplots correspond to the DNS and the constructed pseudo fields, respectively. The black line represents the flame surface in ROM while the red dased line mark the frozen pre-flame region with shared velocity. (For interpretation of the references to colour in this figure legend, the reader is referred to the web version of this article.)

base flow from the DNS results by keeping its pre-flame flow field while removing the thermal expansion of its post-flame velocity field in a physically-consistent manner. Regarding the latter point, it requires the modified post-flame flow to 1) be free of thermal expansion and smoothly connected with the frozen pre-flame flow; 2) lead to a steady G-equation solution that recovers the DNS flame geometry; and 3) represent the original aerodynamic environment around the flame. To enable this, we will rely on an auxiliary simulation.

Specifically, the following procedure is executed. First, select a isotherm line to distinguish with the pre- and post-flame region. Second, directly take the DNS velocity result upstream from the isotherm as the velocity of pseudo base flow in the pre-flame region (this corresponds to the "shared region" in Fig. 2); Third, run a cold-flow simulation on the post-flame domain by solving the DNS model of Eq. (2) without the chemical source terms, using the velocity profile on the isotherm (essentially as a inlet boundary boundary) and the original boundary conditions prescribed to other boundaries. Finally, assign the steady solution of this auxiliary cold-flow simulation as the velocity field of pseudo base flow in the post-flame region. Fig. 2 illustrates the constructed pseudo base flow in (a) along with the original DNS flow in (b) for a M-shape flame configuration. As shown, our result reproduces the correct flame geometry and captures the aerodynamic environment surrounding the flame, while the thermal expansion effect is removed in the post-flame region. Due to model assumption in the G-equation itself, there could be very small difference in the flame position between the steady ROM solution and the DNS result. Lastly, it is important to mention that an selected isotherm contour should be sufficiently close to the flame while at the same time the velocity on that contour line is barely affected by thermal expansion. In practice, we found that the isotherm contour lines, $T = T_u + 10\sim50$ K (T_u is the temperature of unburnt mixture), lead to ideal and similar results. We use $T = T_u + 30$ K for the present study.

2.3. Linear input-output analysis

The input-output analysis [23] is performed to obtain the mode shape of the acoustic-modulated flow field, which is then used to generate the physically-consistent modulation to be superimposed onto the pseudo base flow. This technique should be distinguished from the linear stability analysis purposed to obtain flow eigenmodes. Here the input-output analysis seeks the frequency-domain solution of the linearized Navier-Stokes (LNS) equations but with imposed acoustic perturbations at the inflow boundary. The LNS equations write:

$$i\omega\hat{\rho} + \nabla\cdot(\hat{\rho}\boldsymbol{u}_0 + \rho_0\hat{\boldsymbol{u}}) = 0\,, \tag{4a}$$

$$\rho_0(i\omega\hat{\boldsymbol{u}} + (\hat{\boldsymbol{u}}\cdot\nabla)\boldsymbol{u}_0 + (\boldsymbol{u}_0\cdot\nabla)\hat{\boldsymbol{u}}) = -\nabla\hat{p} + \nabla\cdot\hat{\boldsymbol{\tau}}\,, \tag{4b}$$

$$\rho_0 c_p(i\omega T_0 + \hat{\boldsymbol{u}}\cdot\nabla T_0 + \boldsymbol{u}_0\cdot\nabla\hat{T}) - \nabla\boldsymbol{u}_0 : \hat{\boldsymbol{\tau}}\,, + \hat{\rho}c_p(\boldsymbol{u}_0\cdot\nabla T_0) = \nabla(k\nabla\hat{T}) + \nabla\hat{\boldsymbol{u}} : \boldsymbol{\tau}_0\,, \tag{4c}$$

$$\hat{\rho} = \hat{p}/RT_0 - \rho_0\hat{T}/T_0\,, \tag{4d}$$

$$\hat{\boldsymbol{\tau}} = \mu\left(\nabla\hat{\boldsymbol{u}} + (\nabla\hat{\boldsymbol{u}})^T\right) - 2/3\mu(\nabla\cdot\hat{\boldsymbol{u}})\mathbf{I}\,, \tag{4e}$$

in which the subscript "0" indicates the base-flow quantities and the hat symbol indicates the complex amplitudes of the variables at a given frequency, ω. This set of LNS equations is solved using COMSOL Multiphysics with the steady DNS flame solution as the base flow. It is important to aware that the exothermic effect is accommodated in the base flow and assumed not to significantly impact the flame-upstream acoustic modulation [24]. The LNS based techniques were used to characterize flame responses [13,16]. Differently, our ROM solves the LNS equations in the non-reactive form without the linearized source terms; moreover, rather than directly formulating or evaluating FTFs, the outcome of LNS analysis here is the modulated flow field to evolve the nonlinear

G-equation, from which FDFs/FTFs are then obtained. Also note that the LNS analysis here is performed around a frozen base flow, and therefore the obtain flow reponses are linear modes. It is assumed that flame disturbance does not introduce any feedback influence on the velocity perturbations. This is a key difference from the ROMs in [13,18], where the flame-flow perturbations are directly coupled under certain specific physically-informed mechanisms.

2.4. G-equation and level-set

Once the pseudo base flow and the acoustic-modulation field are obtained. G-equation is solved with the synthesized flow field as illustrated in Fig. 1. The s_L is evaluated with the consideration of flame curvature and flow strain effects. A level-set approach with a fifth-order WENO scheme and a fourth-order RK scheme is used to solve the G-equation. A narrow band technique that only updates the solution in near-flame grid points is employed to reduce the computation cost. In each time step, the scalar field $\mathcal{G}$ is re-initialized to a signed distance function by solving the Eikonal equation to ensure a constant flame thickness, $|\nabla\mathcal{G}|$. In addition, to keep the flame anchored at the burner lip, the $\mathcal{G}$ solution is fixed to zero at the flame-anchoring point. It should be noted here that we solve the G-equation in the nonlinear form. Hence, the proposed ROM can be used to predict both FTF and FDF.

2.5. Model assumptions and limitations

Our ROM has several notable assumptions: *i*) the modulation field is obtained from LNS and therefore, restrictively speaking, the mode shape is only accurate for small perturbation around the base flow; *ii*) the model assumes that the flow response remains linear and the only nonlinearity arises from the flame response; *iii*) unlike in [13,18], the coupled flame-flow feedback effect is not captured in our velocity perturbation field; and *iv*) in the G-equation based kinematic flame model, we assume that the flame is a thin surface and anchored at a point. Regarding the last point, the model error could be reduced by allowing the flame to slide if the detailed information on the motion of the flame base is known from measurements.

3. Validation study

3.1. Flame configuration and simulation setup

We consider the laminar premixed flames in conical and M-shape configurations, experimentally studied by Durox et al. [25], to validate our modeling approach. In their burner setup, the CH4/air mixture with an equivalence ratio of $\phi = 1.08$ is issued from a nozzle of 22 mm in diameter. A rod of 6 mm in diameter is placed at the center of the exit plane, serving as a flame stabilizer. For simplification, the rod is not considered in the calculation for the conical flame. The mean bulk velocity U_0 is 1.96 m/s for the conical flame and 2.12 m/s for the M-shape flame, respectively. In the experiment, the flame is directly situated in ambient air; thus for the simulation we set a slow air coflow at a speed of $2\%U_0$ to ensure the well-posedness. Given the mixture composition and the operating condition ($T_u = 300$ K and 1 atm), the laminar flame speed is $s_L|_{\phi=1.08} = 0.385$ m/s and the thermal flame thickness is about 0.5 mm. In the DNS and ROM calculations, the numerical resolutions around the flame region are $\Delta x = 0.05$ mm and $\Delta r = 0.08$ mm along the streamwise and radial directions, respectively.

3.2. Flame dynamics

Fig. 3 shows the comparison of the instantaneous profiles of modulated flames captured by the experimental measurements [25], the DNS and the ROM. The conical flame is subjected to the perturbation of 102 Hz and amplitude $\hat{u}/U_0 = 26\%$, while the M-shape flame is modulated with the perturbation of 152 Hz and amplitude $\hat{u}/U_0 = 25\%$. Compared to the measurements, the key geometrical features of the flames, such as the flame tip height, flame wrinkle location, and surface topology, are well reproduced in the DNS as well as by the ROM. With regard to the M-shape flame specifically, the inner and outer surfaces show distinct characteristics; and the outer surface situated along the shear layer between the jetting fluid and ambient air exhibits more significant deformation under the modulation. The flame dynamics are further examined at different frequencies, together with the perturbation mode shapes captured via the input-output analysis in Fig. 4. As shown, the axial perturbation mode tends to follow the flame sheet geometry while the radial mode tends to depart from the flame sheet along the axial flow direction. One important finding here is that the vortical mode is substantial only at the flame base for conical flame when realistic gas expansion is considered (here $T_b/T_u = 7$). A similar observation was obtained by Steinbacher et al. [17] who studied a 2D slit flame with a similar gas expansion ratio and decomposed the velocity field into potential and solenoidal parts. Schlimpert et al.'s study [26] also corroborates the present finding, and moreover they found a much stronger impact of vortical mode on flame in the case of negligible thermal expansion. Compared to the conical flame, the M-shape flame seems more receptible to the radial mode due to its distinct flame shape. The radial mode mainly acts on the outer part of the flame and causes large surface distortion, which agrees well with the flame behavior revealed in the experimen-

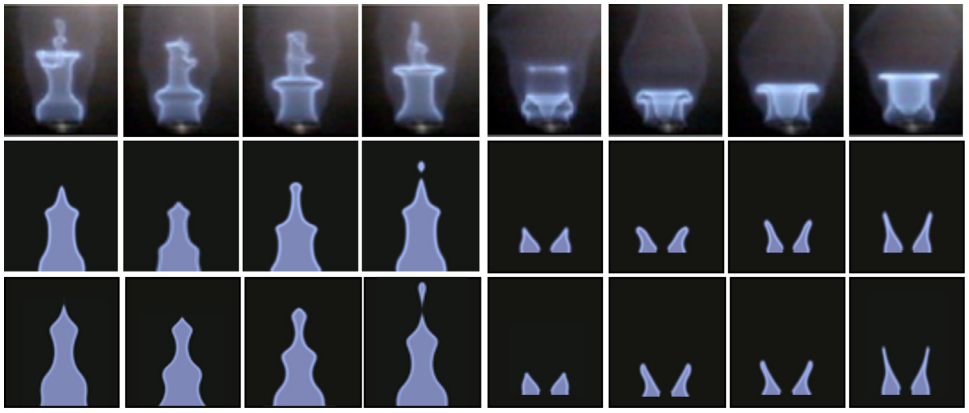

(a) conical flame configuration (b) M-shape flame configuration

Fig. 3. Instantaneous snapshots of acoustically-modulated conical flame (a) at 102 Hz and perturbation amplitude $\hat{u}/U_0 = 26\%$ and M-shape flame (b) at 152 Hz and $\hat{u}/U_0 = 25\%$, captured by the experiment [25] (top row), DNS (middle row), and the proposed ROM (bottom row). The grey regions in DNS and ROM represent the unburnt mixture. The experimental images are taken from [25].

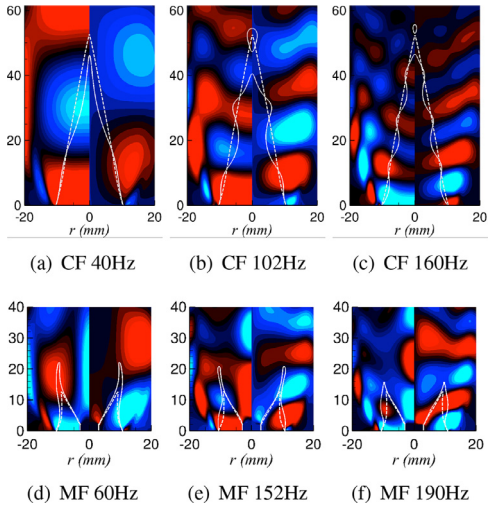

(a) CF 40Hz (b) CF 102Hz (c) CF 160Hz

(d) MF 60Hz (e) MF 152Hz (f) MF 190Hz

Fig. 4. Perturbation mode shapes and instantaneous flame geometries obtained from ROM for conical flame (CF) cases (a-c) and M-shape flame (MF) cases (d-f) at various frequencies. In each panel, left and right half-planes show the streamwise and radial perturbation mode shapes, respectively. The solid and dashed curves denote perturbed and unperturbed flame fronts.

tal images. In addition, the flame tends to be dominated by uniform perturbation at lower frequencies which leads to ampler mode shapes, while by convective perturbation at higher frequencies for which the modal structures become smaller. This observation is also consistent with the previous findings [25,27]. It is proven that the modulation field generated with the proposed method well captures the flow disturbance induced along the shear layer.

3.3. Flame describing function

The comparison of the flame describing functions obtained via the experimental measurements [25], the DNS and the ROM is presented in Fig. 5. It can be seen that both the DNS and ROM accurately capture the gain and phase variations with respect to perturbation frequency and amplitude. The saturation behavior of heat release fluctuation, as well as the rebounds along the gain curves, is well reproduced in the conical flame case; comparatively, the DNS yields slightly improved predictions. For the M-shape flame case, the DNS and ROM also yield similar accuracy in reference with the experimental results. Despite small underprediction in the gain profile over intermediate frequencies, the gain and phase lag behaviors are well captured by the proposed ROM. It is worth noting that the phase lag prediction through G-equation suffered from significant deficiencies [11,15]. The proposed ROM, which is built upon the physically-consistent modulation, provides significant improvement in the phase lag prediction, compared to the previously used ROMs. This aspect will be further elaborated in the next section.

3.4. Assessment of the modulation field

A key aspect of our ROM is that the acoustic modulation field is constructed based on the information derived from the flow physics taking place in the given combustion configuration, and no heuristics are introduced. Developing ROMs

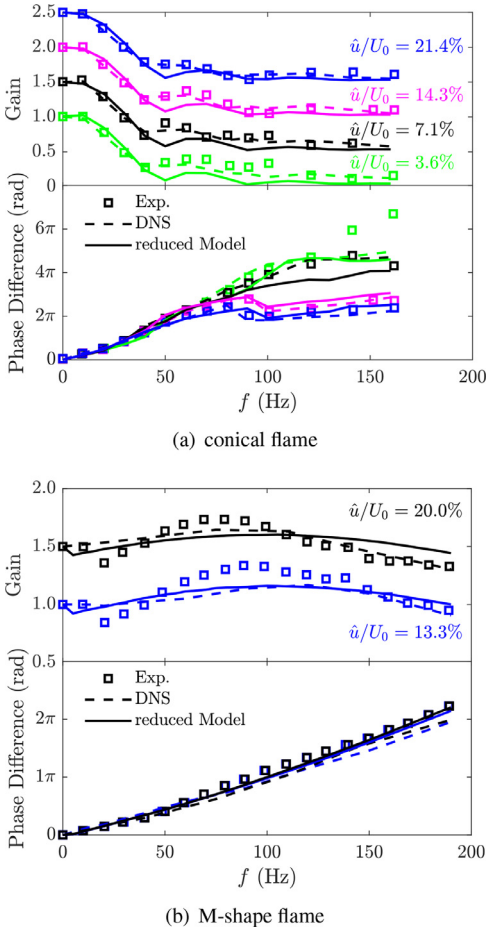

(a) conical flame

(b) M-shape flame

Fig. 5. FDFs of conical flame (a) and M-shape flame (b) obtained from the experiment [25], DNS and the ROM. The curves in the gain plots are shifted by 0.5 for clarity.

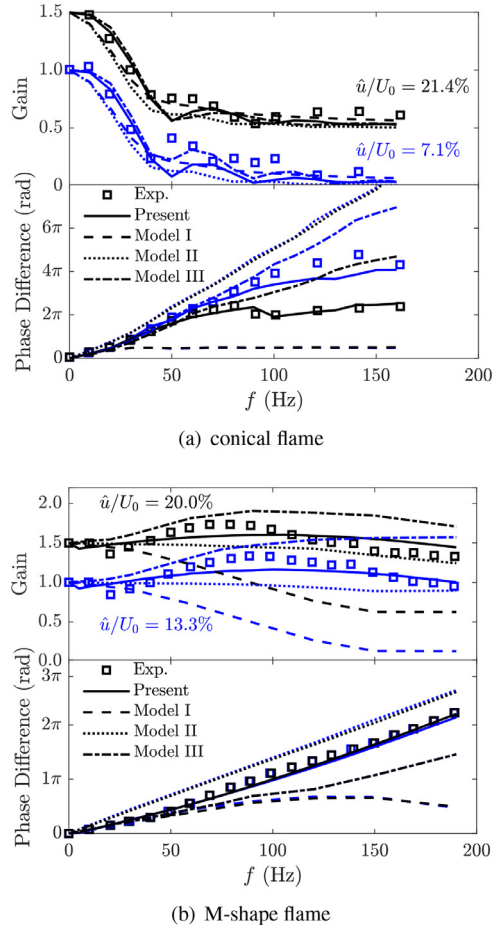

(a) conical flame

(b) M-shape flame

Fig. 6. FDFs of conical flame (a) and M-shape flame (b) obtained from ROM predictions with different modulations. The curves in the gain plots are shifted by 0.5 for clarity.

based on physically-informed velocity perturbations can also be found in the studies of Blanchard et al. [13] and Steinbacher et al. [18]. To assess the modulation field and its role in the ROM, a further investigation is carried out to compare the FDFs predicted with different modulation fields, including those heuristically derived and commonly used in literature. Three modulation models are considered for comparison:

Model I: $u'_x = \hat{u}cos(\omega t),\ u'_r = 0\ ,$

Model II: $u'_x = \hat{u}cos(kx - \omega t),\ u'_r = 0\ ,$

Model III: $u'_x = \hat{u}cos(kx - \omega t),$

$$u'_r = k\frac{r}{2}\hat{u}sin(kx - \omega t),$$

Models I and II represent uniform and convective perturbations [27,28]; and Model III is an improved version of Model II, accounting for the radial perturbation component [29]. In Models II and III, the convective velocity is set to the mean bulk velocity at the nozzle exit. Fig. 6 shows the FDFs predicted with different modulation fields for both conical and M-shape flames. All modulation models lead to reasonably good gain results for the conical flame. The major performance difference lies in the phase-lag prediction. Model I fails in this regard, and Models II and III cannot yield satisfactory phase-lag predictions at high frequencies. Our modulation field offers considerably superior results. As for the M-shape flame, Models I and II fail to capture the amplification effect in the gain profile, and the model performance in phase-lag predictions is similar to that for the conical flame case. This study substantiates that the modulation field constructed via the input-output analysis indeed outperforms the heuristically-presumed modulation fields, and ele-

Table 1
Unperturbed flame heights of confined conical flames obtained in the experiment [31] and by our ROM.

	$C_r = 0.44$	$C_r = 0.66$	$C_r = 0.81$
EXP	42.5 mm	45.6 mm	54.5 mm
ROM	42.9 mm	46.5 mm	57.2 mm

vates the overall fidelity of ROM by serving a key algorithmic ingredient.

4. Application to confined laminar flame

In the previous analysis, the ROM is applied to unconfined laminar flame configurations. In practical scenarios, flames are typically contained in combustors and the confinement effect must be addressed. Hence, further model evaluation is carried out to examine the accuracy of ROM in predicting flame transfer functions for confined laminar premixed flames. For this, we consider the flame configuration of Cuquel et al. [30], in which conical flames are placed in tubes of various radii and flame transfer functions are measured at various confinement ratios (C_r, defined as the ratio of burner-exit radius to the tube radius). For more setup details, the reader is referred to the original paper [30]. We apply the ROM to the flame case with an inflow mass rate of $\dot{m} = 0.566$ g/s which corresponds to $U_0 = 1.32$ m/s. The unperturbed flame heights obtained by our ROM compare well with the experimental measurements, as exhibited in Table 1. The flame shapes, including the perturbed and unperturbed, are illustrated along with the predicted acoustic modulation fields in Fig. 7. There are several key findings. First of all, the stronger confinement leads to longer flame geometry because of the streamwise flow acceleration caused by the enlarged radial flow strain. Our ROM is able to capture this flame behavior; furthermore, the predicted flame (unperturbed) height at each C_r agrees well with the corresponding measurement [30]. Secondly, the flow perturbation modes are significantly altered by confinement. With an increasing C_r, the streamwise mode becomes more elongated and meanwhile the radial mode number reduces. Since the perturbations are convected by the mean flow, these changes in mode shape are a direct result of the growing streamwise mean-flow velocity due to confinement. These mode behaviors are all represented by our ROM. Frequency also plays a role in the mode shape and subsequently the flame behavior. Higher frequency leads to a more rapid decay in mode amplitude along the streamwise direction, as revealed in Fig. 7. The predicted FTFs of the confined flames are compared against the experimental data in Fig. 8. The gain and phase lag predicted by the ROM agree well with those from the measurements [30], espe-

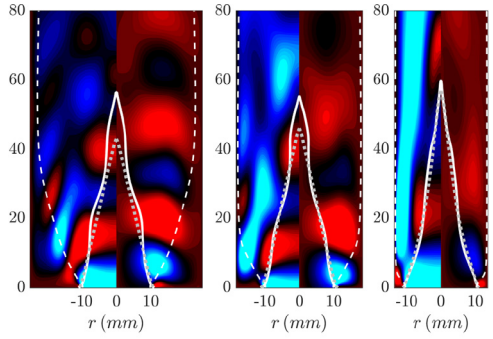

(a) confined conical flames at 65Hz

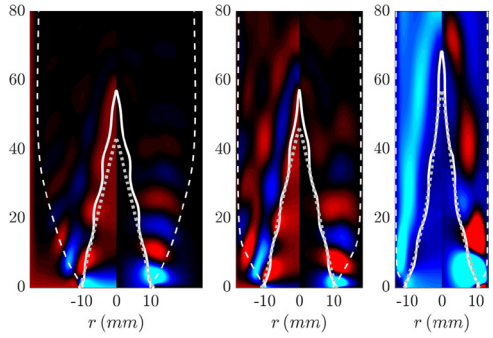

(b) confined conical flames at 115Hz

Fig. 7. Perturbation mode shapes and instantaneous flame geometries obtained from ROM for the confined conical flames at 65 Hz (a) and 115 Hz (b). In each subplot, panels from left and right correspond to $Cr = 0.44,\ 0.60,\ 0.81$, respectively. The left and right half-planes show the streamwise and radial perturbation mode shapes. The plume of burnt gas is indicated by the white dashed line. The solid and dotted curves denote the perturbed and unperturbed flame fronts, respectively.

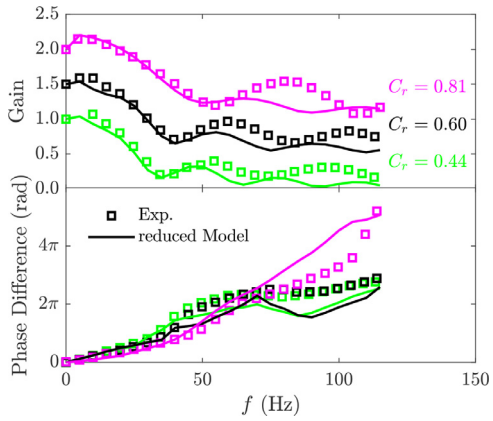

Fig. 8. FTFs of the confined conical flames with different confinement ratios. ROM (line) and experimental (dot) results are both obtained with a modulation level $\hat{u}/U_0 = 10\%$. The experimental data are taken from [30]. The curves in the gain plot are shifted by 0.5 for clarity.

cially in the lower frequency range ($f < 60$ Hz). The overall accuracy is similar to that observed in the unconfined laminar premixed flame configuration, although some discrepancies appear over the rebounds at a higher frequency range. These discrepancies are likely attributed to the feedback effect between flame and flow responses, which is not considered in our ROM. According to the analysis of Steinbacher et al. [18], the gain can be considerably underestimated without accounting for the flame-flow feedback interaction at the higher frequency range. It is noteworthy that the consistent growth of phase lag with respect to frequency is a key feature in the high confinement case ($C_r = 0.81$), different from the saturation behavior in the $C_r = 0.44$ and $C_r = 0.66$ cases. This feature is likely attributed to the peculiar mode shapes created under the strong confinement, and was not addressed by previous modeling effort [30]. It is remarkable that our ROM which is based on the physically-consistent modulation is able to capture the phase-lag behavior in the highly confined flame configuration.

5. Conclusions

We presented a predictive and efficient reduced-order modeling technique for the evaluation of flame describing/transfer functions of laminar premixed flames, in order to facilitate combustion instability analysis. This model is built on the G-equation kinematic model to track flame front and capture flame response to flow modulation. The major innovation is on the construction of a high-fidelity flow field to allow flame evolving in a physically-consistent manner. For this, a pseudo base-flow is first established through a novel approach to replicate the steady-state flame geometry and the corresponding aerodynamic environment; then, a linearized Navier-Stokes input-output analysis is conducted to capture the mode shape of the acoustic-modulation field.

Limitations exist in our ROM. The proposed ROM neglects the flame-flow feedback. Moreover, the ROM implicitly assumes that flow response is triggered around the frozen base flow and remains linear in the perturbed flame field. Hence, model errors appear when the ROM is applied to predict flame response under finite-amplitude acoustic perturbations. The nonlinearity associated with the flame response is captured by the nonlinear G-equation by assuming ideal flame anchoring.

The accuracy of the proposed ROM was assessed in validation studies with the consideration of laminar premixed CH_4/air flames in conical and M-shape geometries. The study shows that the ROM predictions of the flame dynamics and flame describing functions agree well with the experimental measurements and achieve similar accuracy with those obtained from direct numerical simulations. Further investigations highlighted the superiority of the physics-informed perturbation model over the commonly used presumed ones. Lastly, the ROM was applied to flame response predictions for the confined laminar premixed flame to illustrate the generality of the modeling technique and the potential to be used in thermoacoustic analysis of combustors/burners of practical relevance.

Declaration of competing interest

The authors declare that they have no known competing financial interests or personal relationships that could have appeared to influence the work reported in this paper.

Acknowledgments

This work was partially funded bythe NASA EPSCOR Program. We thank the anonymous reviewers who offered us valuable insights and comments.

Supplementary material

Supplementary material associated with this article can be found, in the online version, at doi:10.1016/j.proci.2022.07.229

References

[1] A. Urbano, L. Selle, G. Staffelbach, B. Cuenot, T. Schmitt, S. Ducruix, S. Candel, Exploration of combustion instability triggering using large eddy simulation of a multiple injector liquid rocket engine, Combust. Flame 169 (2016) 129–140.
[2] T. Poinsot, Prediction and control of combustion instabilities in real engines, Proc. Combust. Inst. 36 (1) (2017) 1–28.
[3] A.P. Dowling, A kinematic model of a ducted flame, J. Fluid Mech. 394 (1999) 51–72.
[4] S. Candel, Combustion dynamics and control: progress and challenges, Proc. Combust. Inst. 29 (1) (2002) 1–28.
[5] N. Noiray, D. Durox, T. Schuller, S. Candel, A unified framework for nonlinear combustion instability analysis based on the flame describing function, J. Fluid Mech. 615 (2008) 139–167.
[6] P. Palies, D. Durox, T. Schuller, S. Candel, Nonlinear combustion instability analysis based on the flame describing function applied to turbulent premixed swirling flames, Combust. Flame 158 (10) (2011) 1980–1991.
[7] C.F. Silva, F. Nicoud, T. Schuller, D. Durox, S. Candel, Combining a helmholtz solver with the flame describing function to assess combustion instability in a premixed swirled combustor, Combust. Flame 160 (9) (2013) 1743–1754.

[8] H.J. Krediet, C.H. Beck, W. Krebs, S. Schimek, C.O. Paschereit, J.B.W. Kok, Identification of the flame describing function of a premixed swirl flame from LES, Combust. Sci. Technol. 184 (7–8) (2012) 888–900.
[9] X. Han, A.S. Morgans, Simulation of the flame describing function of a turbulent premixed flame using an open-source LES solver, Combust. Flame 162 (5) (2015) 1778–1792.
[10] X. Han, J. Li, A.S. Morgans, Prediction of combustion instability limit cycle oscillations by combining flame describing function simulations with a thermoacoustic network model, Combust. Flame 162 (10) (2015) 3632–3647.
[11] T. Schuller, S. Ducruix, D. Durox, S. Candel, Modeling tools for the prediction of premixed flame transfer functions, Proc. Combust. Inst. 29 (1) (2002) 107–113.
[12] S. Hemchandra, Premixed flame response to equivalence ratio fluctuations: comparison between reduced order modeling and detailed computations, Combust. Flame 159 (12) (2012) 3530–3543.
[13] M. Blanchard, T. Schuller, D. Sipp, P. Schmid, Response analysis of a laminar premixed m-flame to flow perturbations using a linearized compressible navier-stokes solver, Physics of Fluids 27 (4) (2015) 043602.
[14] A. Orchini, M.P. Juniper, Flame double input describing function analysis, Combust. Flame 171 (2016) 87–102.
[15] B. Semlitsch, A. Orchini, A.P. Dowling, M.P. Juniper, G-Equation modelling of thermoacoustic oscillations of partially premixed flames, Int. J. Spray Combust. Dyn. 9 (4) (2017) 260–276.
[16] A. Avdonin, M. Meindl, W. Polifke, Thermoacoustic analysis of a laminar premixed flame using a linearized reactive flow solver, Proc. Combust. Inst. 37 (4) (2019) 5307–5314.
[17] T. Steinbacher, A. Albayrak, A. Ghani, W. Polifke, Response of premixed flames to irrotational and vortical velocity fields generated by acoustic perturbations, Proc. Combust. Inst. 37 (4) (2019) 5367–5375.
[18] T. Steinbacher, W. Polifke, Convective velocity perturbations and excess gain in flame response as a result of flame-flow feedback, Fluids 7 (2) (2022).
[19] F. Baillot, D. Durox, R. Prud'Homme, Experimental and theoretical study of a premixed vibrating flame, Combust. Flame 88 (2) (1992) 149–168.
[20] A.L. Birbaud, D. Durox, S. Candel, Upstream flow dynamics of a laminar premixed conical flame submitted to acoustic modulations, Combust. Flame 146 (3) (2006) 541–552.
[21] C.D. Pierce, Progress-variable approach for large-eddy simulation of turbulent combustion, Stanford University, 2001 Ph.D. thesis.
[22] J. Li, A.S. Morgans, Feedback control of combustion instabilities from within limit cycle oscillations using $\mathscr{H}_\infty$ loop-shaping and the v-gap metric, Proc. R. Soc. A 472 (2191) (2016) 20150821.
[23] J. Jeun, J.W. Nichols, M.R. Jovanović, Input-output analysis of high-speed axisymmetric isothermal jet noise, Phys. Fluids 28 (4) (2016) 047101.
[24] B. Emerson, T. Lieuwen, M.P. Juniper, Local stability analysis and eigenvalue sensitivity of reacting bluff-body wakes, J. Fluid Mech. 788 (2016) 549–575.
[25] D. Durox, T. Schuller, N. Noiray, S. Candel, Experimental analysis of nonlinear flame transfer functions for different flame geometries, Proc. Combust. Inst. 32 (1) (2009) 1391–1398.
[26] S. Schlimpert, S. Hemchandra, M. Meinke, W. Schroeder, Hydrodynamic instability and shear layer effect on the response of an acoustically excited laminar premixed flame, Combust. Flame 162 (2) (2015) 345–367.
[27] T. Schuller, D. Durox, S. Candel, A unified model for the prediction of laminar flame transfer functions, Combust. Flame 134 (1–2) (2003) 21–34.
[28] T. Lieuwen, Modeling premixed combustion-acoustic wave interactions: a review, J. Propuls. Power 19 (5) (2003) 765–781.
[29] K. Kashinath, S. Hemchandra, M.P. Juniper, Nonlinear thermoacoustics of ducted premixed flames: the influence of perturbation convection speed, Combust. Flame 160 (12) (2013) 2856–2865.
[30] A. Cuquel, D. Durox, T. Schuller, Scaling the flame transfer function of confined premixed conical flames, Proc. Combust. Inst. 34 (1) (2013) 1007–1014.
[31] A. Cuquel, Dynamics and nonlinear thermo-acoustic stability analysis of premixed conical flames, Châtenay-Malabry, École Centrale de Paris, 2013 Ph.D. thesis.